

# Journal of Materials Chemistry A

Accepted Manuscript

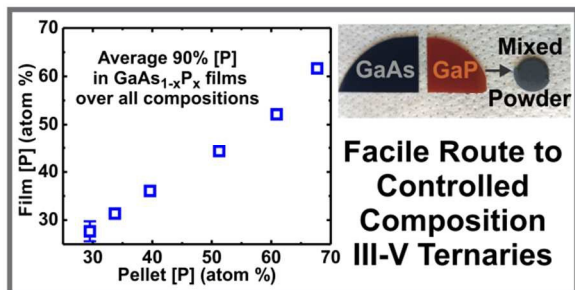


This is an *Accepted Manuscript*, which has been through the Royal Society of Chemistry peer review process and has been accepted for publication.

*Accepted Manuscripts* are published online shortly after acceptance, before technical editing, formatting and proof reading. Using this free service, authors can make their results available to the community, in citable form, before we publish the edited article. We will replace this *Accepted Manuscript* with the edited and formatted *Advance Article* as soon as it is available.

You can find more information about *Accepted Manuscripts* in the [Information for Authors](#).

Please note that technical editing may introduce minor changes to the text and/or graphics, which may alter content. The journal's standard [Terms & Conditions](#) and the [Ethical guidelines](#) still apply. In no event shall the Royal Society of Chemistry be held responsible for any errors or omissions in this *Accepted Manuscript* or any consequences arising from the use of any information it contains.



Close-spaced vapor transport provides  $\text{GaAs}_{1-x}\text{P}_x$  with controlled composition and competitive electronic properties.

## Gallium arsenide phosphide grown by close-spaced vapor transport from mixed powder sources for low-cost III-V photovoltaic and photoelectrochemical devices

Ann L. Greenaway,<sup>a</sup> Allison L. Davis,<sup>b</sup> Jason W. Boucher,<sup>c</sup> Andrew J. Ritenour,<sup>a</sup> Shaul Aloni<sup>d</sup>  
and Shannon W. Boettcher\*<sup>a</sup>

<sup>a</sup>*Department of Chemistry and Biochemistry, University of Oregon, Eugene, Oregon, 97403, USA. Email: [swb@uoregon.edu](mailto:swb@uoregon.edu)*

<sup>b</sup>*Department of Natural and Physical Sciences, Park University, Parkville, Missouri, 64152, USA.*

<sup>c</sup>*Department of Physics, University of Oregon, Eugene, Oregon, 97403, USA.*

<sup>d</sup>*The Molecular Foundry, Lawrence Berkeley National Laboratory, Berkeley, California, 94720, USA.*

### Abstract

We report the heteroepitaxial growth of variable composition  $n$ -GaAs<sub>1-x</sub>P<sub>x</sub> directly on GaAs substrates *via* close-spaced vapor transport using mixed GaAs-GaP powder sources. GaAs<sub>1-x</sub>P<sub>x</sub> films showed an average 10% reduction in atomic concentration of phosphorous from the source material, and ten GaAs<sub>0.7</sub>P<sub>0.3</sub> films were grown with reproducible composition from a single source pellet. Non-aqueous photoelectrochemical measurements were used to assess electronic quality, with the best short-circuit photocurrent of 6.7 mA cm<sup>-2</sup> and open-circuit photovoltage of 0.915 V for  $n$ -GaAs<sub>0.7</sub>P<sub>0.3</sub> with a carrier concentration of  $2 \times 10^{17}$  cm<sup>-3</sup>. The best Hall electron mobility for this composition was 1570 cm<sup>2</sup> V<sup>-1</sup> s<sup>-1</sup>. Cross-sectional transmission electron microscopy of GaAs<sub>0.7</sub>P<sub>0.3</sub> shows single-crystal structure with few defects. We conclude that CSVT is a promising route to the growth of ternary III-V materials like GaAs<sub>1-x</sub>P<sub>x</sub> for low-cost high-efficiency tandem photoelectrochemical or photovoltaic devices.

## Introduction

Improving the cost-performance of solar energy conversion devices such as photovoltaics (PVs) and photoelectrochemical (PEC) water-splitting cells requires advances in deposition technologies to lower cost and improve materials quality. For PVs, advances that decrease the cost per watt of solar power are needed to achieve cost parity with fossil fuels. Increasing energy conversion efficiency (e.g. to  $> 30\%$ ) is perhaps the best route to reducing the cost of PV, because of the substantial “balance of systems” costs that scale with PV device area.<sup>1</sup> For photoelectrochemical water splitting, devices are needed that can generate the required minimum open-circuit voltage of  $\sim 1.7$  V while effectively utilizing the solar spectrum.<sup>2</sup> Tandem architectures employing two semiconductors with different band gaps could be used in both applications. Therefore, inexpensive deposition technologies that produce high-quality semiconductor materials with appropriate band-gaps for tandem devices are needed.

The most-efficient photovoltaic and photoelectrochemical water-splitting devices are based on III-V semiconductors. Many binary III-Vs, including GaAs, have large optical absorption coefficients and direct band gaps, providing for high solar absorption efficiencies in thin films.<sup>3,4</sup> Ternary III-Vs, like  $\text{GaAs}_{1-x}\text{P}_x$ , provide tunable band gaps and lattice parameters which enable multijunction solar PV and water-splitting cells;<sup>5-7</sup> the current record for a three-junction one-sun III-V PV device is  $37.9 \pm 1.2\%$ .<sup>8</sup> III-V tandem cells have also demonstrated record photoelectrochemical (PEC) water splitting efficiencies  $> 12\%$ .<sup>9</sup> However, III-V cells are made with expensive deposition methods, typically metal organic chemical vapor deposition (MOCVD), that lead to estimated cell costs of  $> \$10 \text{ W}_p^{-1}$  even with optimistic cost models.<sup>10</sup> These costs limit terrestrial use of III-Vs to small-area concentrator configurations and precludes use in one-sun applications for PVs<sup>1</sup> and PEC water splitting.<sup>11</sup> If tandem devices incorporating

III-Vs are to be used for one-sun PV or PEC applications, an improved low-cost production method is needed to compliment strategies for reducing current substrate costs.

Close-spaced vapor transport (CSV T) is a method for depositing high-quality III-V semiconductor epilayers at ambient pressure from a solid source.<sup>12,13</sup> The reactor is shown schematically in Figure 1. Either a halide species or water vapor is diluted in H<sub>2</sub> to act as a transport agent for the reactive precursor species, which is generated by the decomposition of the higher-temperature source. The reactive species deposits at the cooler substrate after diffusion across a gap, typically  $\leq 1$  mm. We showed that CSV T can produce *n* and *p*-GaAs from deliberately doped powder sources with Hall mobilities comparable to those of MOCVD-grown material over a wide range of dopant densities, using water vapor as a transport agent.<sup>14</sup> We fabricated the first CSV T-grown GaAs homojunction solar cells, with open-circuit potentials ( $V_{OC}$ ) over 900 mV and internal quantum efficiencies ( $\Phi_{int}$ ) of  $\sim 90\%$  for unpassivated devices.<sup>15</sup> Although the overall device efficiency ( $\eta$ ) was only  $\sim 8\%$ , device physics models show that cells fabricated using CSV T could achieve  $\eta > 24\%$  with surface passivation and anti-reflective coatings.<sup>16</sup> We previously demonstrated *n*-GaAs photoelectrodes with efficiencies nearing those of photoelectrodes grown using MOCVD. Finally, the growth rate of CSV T (we typically use up to  $\sim 400$  nm min<sup>-1</sup>, but faster is possible) can exceed that of MOCVD and MBE (typically  $\mu\text{m hr}^{-1}$ ).<sup>7,17,18</sup> If such materials control could be extended to ternary III-V semiconductors with tunable band gaps, it would make CSV T attractive for low-cost tandem cell fabrication for either PV or PEC water splitting.

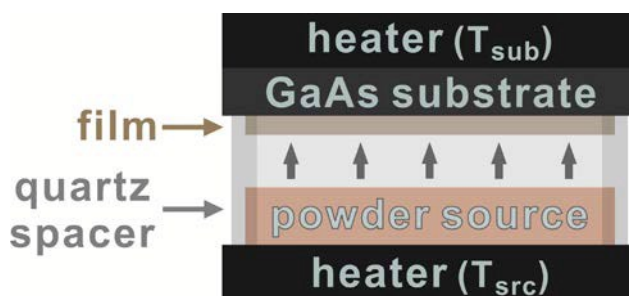
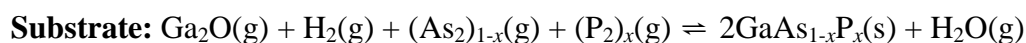
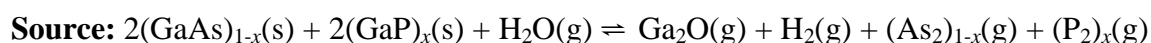


**Figure 1:** Schematic representation of the CSVT reactor. For III-V growth,  $T_{src} > T_{sub}$ . Transport agent flow, Si spacers between the heaters and source/substrate, and the surrounding quartz tube have been omitted for clarity.

$\text{GaAs}_{1-x}\text{P}_x$  in particular is a useful target ternary III-V for PV and PEC applications. For  $[\text{P}] = 30\%$  of the total group V concentration (i.e.  $x = 0.3$ ), it has a direct band gap  $E_g \approx 1.8$  eV. This band gap is ideal for the top cell in a  $\text{GaAs}_{1-x}\text{P}_x/\text{Si}$  one-sun tandem PV or PEC water splitting device, providing theoretical limiting efficiencies of  $37\% - 45\%$ <sup>19,20</sup> and  $\sim 24\%$ <sup>21,22</sup> respectively. For  $[\text{P}] \geq 44\%$ ,  $\text{GaAs}_{1-x}\text{P}_x$  with a larger, indirect band gap might be used as a window layer on a GaAs homojunction solar cell if interface defects could be managed. Historically, however,  $\text{GaAs}_{1-x}\text{P}_x$  has largely been used in photodiodes and LEDs.<sup>23,24</sup> It has found limited application in PV in part because of difficulty with growth by MOCVD. The group V precursor decomposition rates differ dramatically at the growth temperatures for multijunction solar cells, requiring a large excess of P precursor to achieve the desired film composition.<sup>25,26</sup>

$\text{GaAs}_{1-x}\text{P}_x$  can be deposited by CSVT from a source of mixed GaAs and GaP powders.<sup>13,27-29</sup> The reaction with water vapor occurs as follows:<sup>29,30</sup>



The supersaturation of the gas-phase reactants at the substrate are controlled by varying the source-substrate temperature difference ( $\Delta T$ ).<sup>13,31,32</sup> *In situ* generation of the reactive species requires only a carrier gas ( $\text{H}_2$ ) and a transport agent ( $\text{H}_2\text{O}$ ), eliminating the need for the complex

mix of toxic and pyrophoric gaseous precursors used in MOCVD production of  $\text{GaAs}_{1-x}\text{P}_x$ ,<sup>25</sup> thus reducing hazards and potential cost. CSVT operates at atmospheric pressure, rather than the lower pressures sometimes employed in MOCVD<sup>24,33</sup> or the high vacuum conditions of MBE. There is no need to crack the P precursor as would be typical in molecular beam epitaxy, an alternative, slower growth method.<sup>34</sup> Additionally, CSVT processes have reported > 95% source utilization.<sup>12</sup>

Both water vapor<sup>28,29</sup> and halides<sup>35</sup> have been used as transport agents for  $\text{GaAs}_{1-x}\text{P}_x$  growth in CSVT. Source materials included mechanically ground GaAs and GaP<sup>28,35</sup> and melt-grown  $\text{GaAs}_{1-x}\text{P}_x$ .<sup>28</sup> The reports of Gottlieb and of Purohit explored both composition and growth rates but reported no electronic characterization.<sup>28,29</sup> Hoss et al. provide, to our knowledge, the only electronic characterization of  $\text{GaAs}_{1-x}\text{P}_x$  produced by CSVT, of  $p^+$ - $\text{GaAs}_{1-x}\text{P}_x$  with [P] = 20% and a low Hall mobility  $\mu_h = 30 \text{ cm}^2 \text{ V}^{-1} \text{ s}^{-1}$ .<sup>35</sup> While these studies show that  $\text{GaAs}_{1-x}\text{P}_x$  growth is feasible using CSVT, comprehensive studies of the crystalline and electronic properties of films grown by this method are not available.

Herein we report the growth and characterization of  $n$ - $\text{GaAs}_{1-x}\text{P}_x$  epilayers,  $25\% \leq [\text{P}] \leq 65\%$ , directly on single-crystal GaAs substrates from combined powder sources using CSVT. High-resolution x-ray diffraction measurements indicate that the  $\text{GaAs}_{1-x}\text{P}_x$  films grow epitaxially on the GaAs substrates over the range of [P], and that mixed GaAs-GaP powder sources yield  $\text{GaAs}_{1-x}\text{P}_x$  films with an average 10% reduction in [P] from the pellet content, an apparent improvement over other  $\text{GaAs}_{1-x}\text{P}_x$  growth methods which require large excesses of P precursor. Non-aqueous photoelectrochemical measurements show good photoresponse for all  $\text{GaAs}_{1-x}\text{P}_x$  compositions, and optimization of  $\text{GaAs}_{0.7}\text{P}_{0.3}$  growth conditions gave  $J_{\text{SC}} = 6.7 \text{ mA cm}^{-2}$  and a Hall mobility  $\mu_e = 1570 \text{ cm}^2 \text{ V}^{-1} \text{ s}^{-1}$ , suggesting that with further optimization these

films could be useful for high-efficiency tandem devices – especially if growth on Si bottom cells becomes feasible.

## Experimental Methods

### *GaAs<sub>1-x</sub>P<sub>x</sub> film growth*

Powder sources for GaAs<sub>1-x</sub>P<sub>x</sub> films were prepared using the method described by Ritenour *et al.* for doped GaAs sources.<sup>14</sup> The appropriate ratios of GaAs and GaP were ground separately in an agate mortar and pestle (total mass ~400 mg), then combined and pressed in a 13 mm pellet die at 35 mPa. Nominally undoped GaAs wafers (AXT, Inc.) were used for all powder sources. For the varied composition series sources, a GaP wafer, S-doped with  $N_D = 1.4 \times 10^{18} \text{ cm}^{-3}$  (University Wafer) was used, while an undoped GaP wafer (MTI Corp.) was used for the varied temperature series source. The mortar and pestle were cleaned by etching in NH<sub>4</sub>OH and H<sub>2</sub>O<sub>2</sub>, then rinsing with 18.2 MΩ-cm water. <100>-oriented single-crystal GaAs wafers (AXT, Inc.), Si-doped with  $N_D = 1 \times 10^{18} \text{ cm}^{-3}$  (for PEC measurements) or nominally undoped (for Hall effect measurements), were used as substrates. These were etched with 10:1:0.5 H<sub>2</sub>O:NH<sub>4</sub>OH:H<sub>2</sub>O<sub>2</sub> for 30 s, rinsed with 18.2 MΩ-cm water and HPLC-grade isopropanol, and spun dry before growth.<sup>15,36</sup>

Detailed information on the CSVT reactor has been reported previously.<sup>14-17</sup> The source and substrate were heated using resistive graphite heaters. The source ( $T_{\text{src}}$ ) and substrate ( $T_{\text{sub}}$ ) temperatures were set using PID controllers and monitored throughout each growth to maintain their temperature difference,  $\Delta T$ , using type-K thermocouples embedded in the heaters. A quartz ring with 14 mm inner diameter, 1.4 mm thick, was used as a spacer, providing a 0.7 mm space between source and substrate. H<sub>2</sub> (Praxair, research grade) was used as a carrier gas. The transport agent was 18.2 MΩ-cm H<sub>2</sub>O introduced at ~2500 ppm during growth. Before growth,

the chamber was evacuated using a Pfeiffer Vacuum HiCube turbo pump, refilled with dry H<sub>2</sub>, and purged until [H<sub>2</sub>O] was ~ 50 ppm. The source and substrate heaters were ramped to their final temperatures under dry H<sub>2</sub>. Wet H<sub>2</sub> flow was initiated and growth temperatures were maintained for 20 min. Then wet H<sub>2</sub> flow was stopped and the reactor was allowed to cool under dry H<sub>2</sub> and subsequently under Ar.

Two series of samples were produced for this study. For the varied composition series, a range of P concentrations (atom %) was investigated using pressed powder sources with 30% ≤ [P] ≤ 70% (Table S1). For the varied temperature series, a single pellet with [P] = 30% was used as a source. The five composition series samples were grown using a single set of growth parameters, with  $T_{\text{src}} = 900$  °C. The ten temperature series samples were grown at a range of source temperatures of  $800$  °C ≤  $T_{\text{src}} \leq 950$  °C. In all cases,  $\Delta T = 20$  °C. After growth, film thicknesses were measured using a Zygo 7300 optical profilometer.

### *Materials characterization*

For high-resolution X-ray diffraction (XRD), a Rigaku SmartLab X-ray diffractometer equipped with a Ge (220) × 2 monochromator and  $R_x R_y$  tilt stage was used for coupled  $\omega/2\theta$  scans. The beam was aligned to the substrate by setting  $2\theta$  to the Bragg condition for the [004] reflection of GaAs and rocking the stage angle  $\omega$  to find the maximum intensity. A scan of  $2\theta$  over the region of interest was used to identify the GaAs<sub>1-x</sub>P<sub>x</sub> [004] peak, then  $\omega$  was scanned with  $2\theta$  set to the Bragg condition for the GaAs<sub>1-x</sub>P<sub>x</sub> [004] peak to obtain rocking-curve full-width at half-maximum (FWHM) values. For energy dispersive spectroscopy (EDS), an Oxford Instruments X-Max<sup>N</sup> 50 silicon drift detector was used. Elemental maps showed that the films were homogeneous; the composition of each film was determined by averaging [P] at three locations. Plan-view and cross-sectional scanning electron microscopy (SEM) was conducted

using a FEI Helios Dual Beam, which was also used to produce the cross-section for high-resolution transmission electron microscopy (HR-TEM). The SEM working distance was 4 mm and the accelerating voltage was 5 kV; the TEM was a JEOL 2100F operating at an accelerating voltage of 200 kV.

For the temperature series, the composition of the source pellet was monitored using wavelength-dispersive X-ray fluorescence (XRF). After pressing, the pellet was sintered in the CSVT under dry H<sub>2</sub> at 800 °C for 5 minutes with  $\Delta T = 0$ . Following this step, Ga, As, and P contents were measured using a sequential wavelength-dispersive XRF spectrometer (Rigaku ZSX Primus II) before every growth in the temperature series; measurements were repeated six times. After completing the growths, powder XRD  $\theta/2\theta$  scans with Bragg-Brentano focusing were used to identify the phases present in the source pellet.

Time-of-flight secondary ion mass spectrometry (TOF-SIMS) negative spectra were measured using an ION-TOF mass spectrometer with Bi<sup>3+</sup> analysis gun and Cs<sup>+</sup> sputter gun. Relative sensitivity factors were used to convert ion counts to bulk dopant densities:<sup>14</sup>

$$[E] = RSF_E \times \frac{I_E}{I_M} \quad (1)$$

where  $[E]$  is the concentration (cm<sup>-3</sup>) of the analyte element,  $RSF_E$  is the relative sensitivity factor for that element in a GaAs matrix from literature,<sup>37</sup>  $I_E$  is the total ion count for the analyte and  $I_M$  is the total ion count for the matrix. For this study, RSF values were referenced to Ga rather than As or P to ensure that samples with different  $[P]$  were directly comparable.

#### *Photoelectrochemical and electronic characterization*

GaAs<sub>1-x</sub>P<sub>x</sub> photoelectrodes were constructed according to established methods.<sup>14,17</sup> Ohmic contacts were made using either AuGe (100 nm, diffused at 450 °C for 90 s in 5% H<sub>2</sub>/95% N<sub>2</sub>) or

InGa (scribed, diffused at 450 °C for 10 min in 5% H<sub>2</sub>/95% N<sub>2</sub>). Electrodes were constructed by attaching tinned-copper wire to the samples using silver paint (Ted Pella 16040-30) and feeding the wire through glass tubing. The samples were enclosed to a surface area between 0.02 and 0.05 cm<sup>2</sup> with non-conductive epoxy (Loctite Hysol 1C and 9460). The geometric surface areas of the final electrodes were measured using a digital scanner and ImageJ software.

PEC *J-E* measurements were conducted as previously reported.<sup>17,38</sup> The GaAs<sub>1-x</sub>P<sub>x</sub> electrodes were submerged in an electrolyte of 100 mM sublimed ferrocene and 0.5 mM recrystallized ferrocenium in dry acetonitrile with 1 M LiClO<sub>4</sub> (Alfa Aesar, 99%) as the supporting electrolyte. Measurements were conducted on a Biologic potentiostat in three-electrode mode under AM 1.5G solar simulation (Abet Technologies 10500) at 20 mV s<sup>-1</sup> scan rate. The counter electrode was a Pt mesh and the reference electrode was a Pt wire poised at the solution potential and positioned ~5 mm from the working electrode surface to minimize uncompensated series resistance.

Impedance spectroscopy was conducted in the same electrochemical solution in the dark using a DC reverse bias between 0 and 1 V in 10 steps with a 10 mV AC bias amplitude. Measurements which resulted in linear Bode plots and phase angles near -90° over a large range of frequencies were fit to an equivalent circuit to determine the capacitance of the depletion region as a function of working electrode bias (the circuit and details of the fit procedure have previously been reported).<sup>14,17</sup> Equation 2 was used to determine the dopant density,  $N_D$ , and the flat band potential  $V_{bi}$ ,<sup>39</sup> while equation 3 was used to determine the depletion width  $W$ :<sup>40</sup>

$$\frac{1}{C^2} = \frac{2(V_{bi} - V_{app} - \frac{kT}{q})}{q\epsilon N_D A^2} \quad (2)$$

$$W = \sqrt{\frac{2\epsilon}{qN} (V_{bi} - V_{app} - \frac{kT}{q})} \quad (3)$$

where  $\varepsilon$  is the dielectric constant,  $q$  is the fundamental charge,  $V_{app}$  is the applied bias relative to solution potential,  $k$  is the Boltzmann constant, and  $T$  is room temperature.

Three films from the temperature series ([P] = 30%) were deposited on semi-insulating GaAs substrates as described above with  $T_{src} = 900$  °C and  $\Delta T = 20$  °C. These films were then cut into squares and ohmic contacts were made to the corners using annealed AuGe eutectic. Hall effect measurements were made on a lab-built system at 300 K with fields between 0 and 10 kG. The majority carrier mobility  $\mu_e$  was measured using the Van der Pauw method,<sup>41</sup> which also was used to determine the carrier concentration,  $N_D$ , of the films.

### *Reflectivity and Spectral Response*

The reflectance  $R(\lambda)$  of each sample was measured using a Perkin Elmer Lambda 1050 spectrometer with an integrating sphere.<sup>38</sup> Samples were measured in air|sample and air|glass|acetonitrile|sample configurations to account for reflection losses in the PEC spectral response measurements. Due to inhomogeneity in surface roughness of the samples, the reflectance varied between samples; however, all samples displayed peak shapes indicative of their intermediate compositions between GaP and GaAs (Figure S3).

A Bentham PVE300 system was used to measure the spectral response of the photoelectrochemical samples. Monochromatic light was chopped at 35 Hz and the signal was measured using a lock-in amplifier. For these measurements, a two-electrode short-circuit PEC configuration was used and the ferrocene/ferrocenium electrolyte was diluted to reduce parasitic light absorption. A Bentham 11677 calibrated photodiode was used to determine incident light intensity at each wavelength so the nA-range signal could be converted to external quantum efficiency ( $\Phi_{ext}$ ). Additional experiments, described in the SI, were used to confirm that no artifacts affected the measured short-circuit current (Figure S4).

## Results and Discussion

### *Sample Growth, Phosphorous Characterization, and Crystalline Quality*

Two series of GaAs<sub>1-x</sub>P<sub>x</sub> films were produced to determine the effects of source composition and growth temperatures on GaAs<sub>1-x</sub>P<sub>x</sub> deposition by CSVT. Although single-crystal GaAs and GaP wafers were ground and used as powder sources in this study, should the CSVT process be commercialized it is anticipated that directly prepared powders (with cost at scale approaching that of the bulk elements) would be used as precursors. For the varied composition series, high growth temperatures (compared to CSVT GaAs growth)<sup>14-18</sup> were used based on literature reports that temperatures above 900 °C are required for efficient P incorporation.<sup>28,29,35</sup> All growths resulted in films with non-specular surfaces (samples C1-C5). Film compositions were determined using  $P/(P+As)$  via EDS (Figure 2A).<sup>42</sup> The GaAs<sub>1-x</sub>P<sub>x</sub> (004)  $\theta/2\theta$  peak position (Figure 2B) was also used with Vegard's law to calculate [P] from the lattice parameter.<sup>3</sup> By XRD, [P] of the films averaged ~90% of [P] for the sources, which is in good agreement with the reports of GaAs<sub>1-x</sub>P<sub>x</sub> growth from Gottlieb and Purohit, who both observed a similar reduction in [P] from source to substrate. However, the non-specular surfaces grown at these conditions differ from Gottlieb's report of mirror-like surfaces for most growths, which may be due to the use of a GaAs<sub>1-x</sub>P<sub>x</sub> wafer rather than mixed powder for a source material (Purohit does not describe the GaAs<sub>1-x</sub>P<sub>x</sub> surface morphology).<sup>28,29</sup> Compositions of the source pellets and films as well as film thicknesses for the composition series can be found in Table S1.

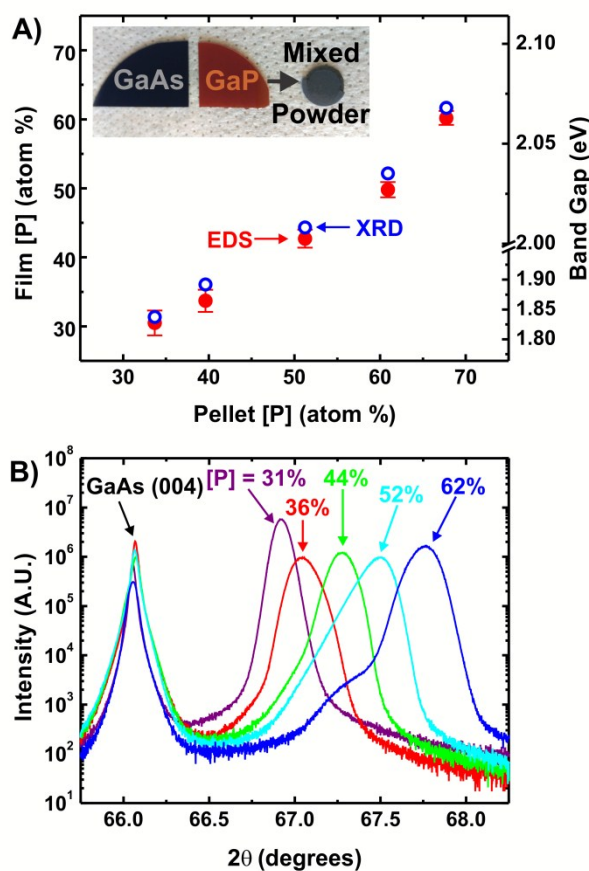


**Figure 2:** **A)** The initial pellet source and final film compositions of the composition series of GaAs<sub>1-x</sub>P<sub>x</sub> films. The second y axis shows the expected  $E_g$  of these samples based on [P]. Images of the source wafers and a pellet are inset. **B)** XRD scans of the five composition series samples, showing the shifting position of the GaAs<sub>1-x</sub>P<sub>x</sub> (004) peak with increasing [P] compared to the GaAs substrate (004) peak.

The high incorporation of P (with only a 10% reduction from source to film across the series) in the composition series samples is in contrast to GaAs<sub>1-x</sub>P<sub>x</sub> growth in MOCVD and MBE. Unlike MOCVD and MBE, the P precursor in CSVT does not require cracking to produce the active species,<sup>26,34</sup> and no overpressure of either group V element compared to the group III element is required for deposition, as in MOCVD (where typical growth conditions use at least threefold and often more than tenfold excess group V precursor).<sup>43</sup> For a completely enclosed CVST growth zone, the utilization of both group III and V elements should approach 100%.<sup>12,28</sup> This is a key difference from gas-phase deposition technologies, like MOCVD, which rely on

gas flow for deposition and thus typically utilize only ~30% of the more-expensive group III element.<sup>10</sup> However, we did observe qualitatively that phosphorous was lost from the reaction zone in the CSVT more quickly than arsenic, as evidenced by a reddish coating in the CSVT downstream of the heaters. This is likely due to the higher diffusivity of  $P_2$  relative to  $As_2$  and thus faster transport out of the incompletely sealed reaction zone. This loss explains the small reduction in [P] of the films relative to their sources, and likely was the cause of the [P] reduction in the final film observed in previous CSVT growths.<sup>28,29</sup>

XRD analysis of a source pellet with [P] = 30% after several growths shows that the GaP and GaAs formed a  $GaAs_{0.7}P_{0.3}$  ternary powder (Figure S1). Because the transport reactions at the source and substrate (shown above) are each at near-equilibrium during the CSVT growth process and the growth rate is controlled by diffusion in the reaction zone,<sup>44</sup> it is likely that the substrate follows the average source composition because the GaAs and GaP are alloying, at least at the surface, during heating, even during the first growth from a pellet. Thus, the partial pressures of P and As at the source are not set by the individual GaAs and GaP phases, but rather by the alloyed source material. Further studies are needed to fully elucidate the details of ternary growth by CSVT.

Despite their non-specular surfaces, diffraction analysis shows that all films in the composition series are epitaxial and aligned to the  $\langle 100 \rangle$  GaAs surface (Figure 2B). Some compositional inhomogeneity is evident from diffraction in all of the films, except sample C1 ([P] = 31%). Based on the small lower-angle shoulder observed on each  $GaAs_{1-x}P_x$  (004) peak these inhomogeneities are minor. Crystalline quality was assessed qualitatively from the full width at half maximum (FWHM) of the  $GaAs_{1-x}P_x$  (004) rocking-curve  $\omega$  peak for each film (Figure 3). All films showed larger FWHM than the substrate indicating a larger number of

dislocations in these films than the GaAs substrate, consistent with the significant lattice mismatch between GaAs and the  $\text{GaAs}_{1-x}\text{P}_x$  compositions studied here.

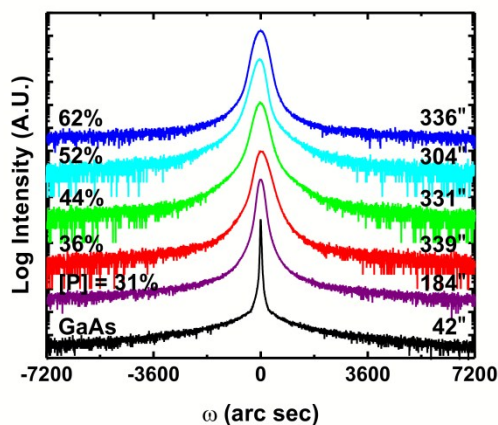


**Figure 3:** Rocking curve ( $\omega$ ) scans of each  $\text{GaAs}_{1-x}\text{P}_x$  (004) peak for the composition series. Note the large FWHM of all films compared to a GaAs substrate caused in part by misfit dislocations on the lattice mismatched substrate.

A second series of samples were grown to investigate the effect of growth temperature on P incorporation in CSVT  $\text{GaAs}_{1-x}\text{P}_x$  and to quantify the change in [P] of the source over multiple uses (samples T1-T10).  $T_{\text{src}}$  was varied between 800 and 950 °C while  $\Delta T$  was held constant at 20 °C (i.e. for  $T_{\text{src}} = 900$  °C,  $T_{\text{sub}} = 880$  °C). The initial source composition was [P] = 30%. Like the films in the composition series, these temperature series samples were found to be epitaxial and aligned to their GaAs substrates (Figure 4A). The tight clustering of the  $\text{GaAs}_{1-x}\text{P}_x$  (004) peaks despite differences in temperature indicates that growth temperature has little impact on P incorporation in the epilayer and that the difference between source and film [P] described above is likely solely due to precursor escape from the reaction space. With the exception of the first film (discussed below), the films with repeated growth parameters ( $T_{\text{src}} = 900$  °C) show reproducible P incorporation. The limited deviation in [P] of the other films indicates that, for the temperature range investigated, growth temperature does not play a large role in determining P incorporation in the film. The growth temperatures, [P], change in [P] from the source, and film

thickness are shown in Table 1. In addition to [P], film thicknesses, and growth rates of the samples grown at  $T_{\text{src}} = 900$  °C are reproducible. For the other films, the highest growth temperature ( $T_{\text{src}} = 950$  °C) resulted in the highest growth rate and thickest film, while lower growth temperatures resulted in thinner films, consistent with an increased reaction rate at higher temperature. The rocking curves for these samples show FWHM values (Figure 4B) which follow the trend of the measured film thicknesses, with the lowest FWHM for the thickest sample, grown at  $T_{\text{src}} = 950$  °C, and the largest FWHM for the sample grown at  $T_{\text{src}} = 800$  °C.

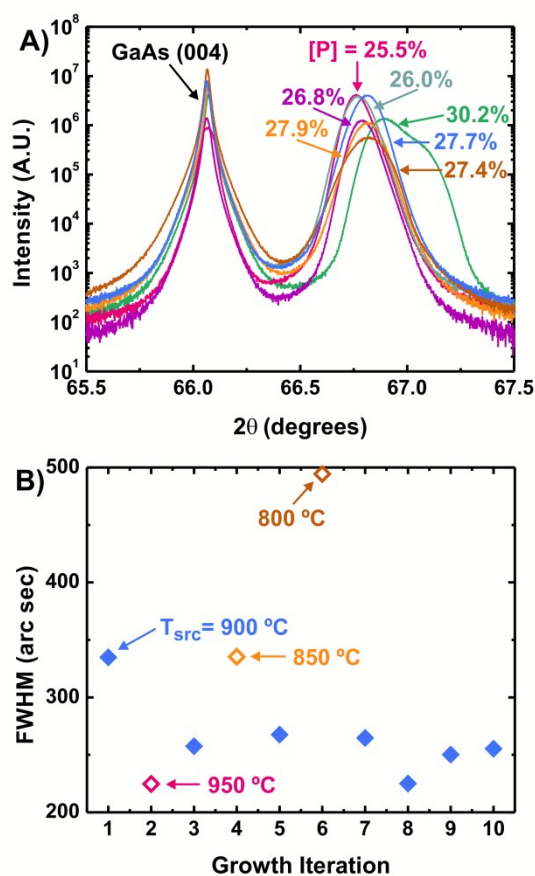


**Figure 4:** A) XRD scans of the first seven samples of the temperature series (T8-T10 omitted for clarity). Note the compositional inhomogeneity in sample T1, [P] = 30.2%. B) FWHM values for the temperature series, which correlate strongly with growth temperature and therefore film thickness.

**Table 1:** Temperature series film data

Sample	T <sub>src</sub> (°C)	Film [P] by XRD (atom %)	Difference from source (%)	Film Thickness (μm)
T1	900	30.2	2.3	4.9 ± 0.7
T2	950	25.5	13.4	8.7 ± 1.6
T3	900	26.8	9.3	4.4 ± 0.4
T4	850	27.9	5.4	1.9 ± 0.2
T5	900	26.0	11.8	3.8 ± 0.5
T6	800	27.4	7.0	1.2 ± 0.5
T7	900	27.7	6.2	4.1 ± 0.3
T8	900	28.1	4.5	3.8 ± 0.6
T9	900	27.5	6.7	4.2 ± 1.0
T10	900	27.7	6.1	4.4 ± 0.6

In order to achieve high materials utilization over the lifetime of a source, its composition should remain constant. Preferential depletion of one group V element over the other would cause [P] and therefore  $E_g$  in the resulting films to drift from the desired composition. XRF was used to qualitatively examine the change in [P] of the source pellet. After pressing, the temperature series source pellet was briefly sintered under H<sub>2</sub> to improve its structural integrity as described in the experimental methods. Its composition was then measured before each of the ten growths. The [P] of the pellet and each film (from XRD) can be seen in Figure 5. There is significant depletion of P after the first growth from the front of the pellet, which is reflected in the higher [P] of the first sample of this series (sample T1, [P] = 30.2%). T1 also shows compositional inhomogeneity, as evidenced by the shoulder at higher angles in the diffraction analysis representing P-rich components (Figure 4A). Subsequent growths show no such inhomogeneity. These results suggest that sintering at 900 °C is sufficient to drive the alloying of the GaAs and GaP in the source material to provide a homogeneous source vapor. Compositional inhomogeneity of the partially sintered pellet likely contributed to the low crystalline quality of the first sample.

After the first growth, the P content of the source is stable over the course of the temperature series growths, as it is in the resulting films. However, [P] of the source was lower

than that of the films, suggesting depletion of P at the surface of the pellet. Because XRF does not probe the entire film, the backside of the pellet was measured after T7 to determine if P depletion was occurring uniformly throughout the pellet (Figure 5). The results show that more P remains in the whole pellet while the surface closest to the substrate is depleted. Nonetheless, the resulting film composition was reproducible. As mentioned above, a powder XRD scan of the temperature series pellet after the growths confirmed that the pellet had sintered into a solid solution (Figure S1).

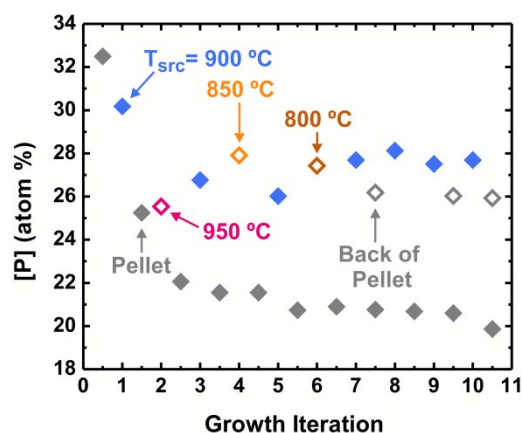


**Figure 5:** Evolution of the [P] in the temperature series pellet source and the resulting ten films. Films grown at different  $T_{src}$  are indicated.

Plan-view scanning-electron micrographs of all  $\text{GaAs}_{1-x}\text{P}_x$  films showed a high prevalence of irregular microstructures and surface texturing (Figure 6). The rough surfaces are likely a result of the tensile strain imposed on the  $\text{GaAs}_{1-x}\text{P}_x$  films by growing on a mismatched substrate and appear similar to, if much rougher than, the cross-hatched surface morphology observed when compositionally graded buffer layers are used.<sup>45</sup> Adventitious microstructures (Figure 6A, arrows) on the films are likely due to particles transferring from the powder source, and have been separately observed in CSVT GaAs grown from pellet sources in this system. The temperature series samples allowed for characterization of the particulate transfer from a pellet

over time. Although there are many microstructures observed on the first sample (Figure 6A), by the tenth and final growth from the pellet, they were almost entirely eliminated (Figure 6B). These data suggest that after sufficient sintering (which could be done prior to initial film growth), the source pellets no longer contain particulates sufficiently small to transport during the CSVT process. To further probe the crystal quality of the CSVT  $\text{GaAs}_{1-x}\text{P}_x$ , a TEM cross-section was prepared using focused ion beam milling of sample T10 (Figure 7). HR-TEM confirms the finding from XRD that the film is an epitaxial single crystal. Notably, there is a very low incidence of defects throughout the sample and the cross-section appears uniform.

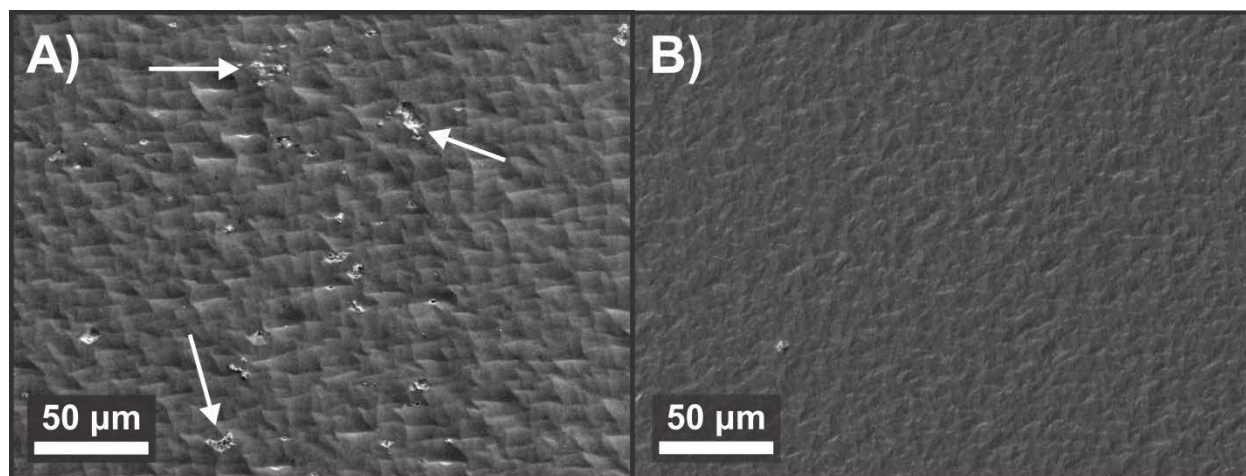


**Figure 6:** Representative plan-view SEM images of the temperature series  $\text{GaAs}_{1-x}\text{P}_x$  surfaces. **A)** Sample T1 ([P] = 30.2%), showing adventitious microstructures, some of which are indicated by white arrows, and a large degree of surface texturing. **B)** Sample T10 ([P] = 27.7%), where the microstructures are no longer observed. SEMs of the composition series samples, which show more microstructures and texturing, can be seen in Figure S2.

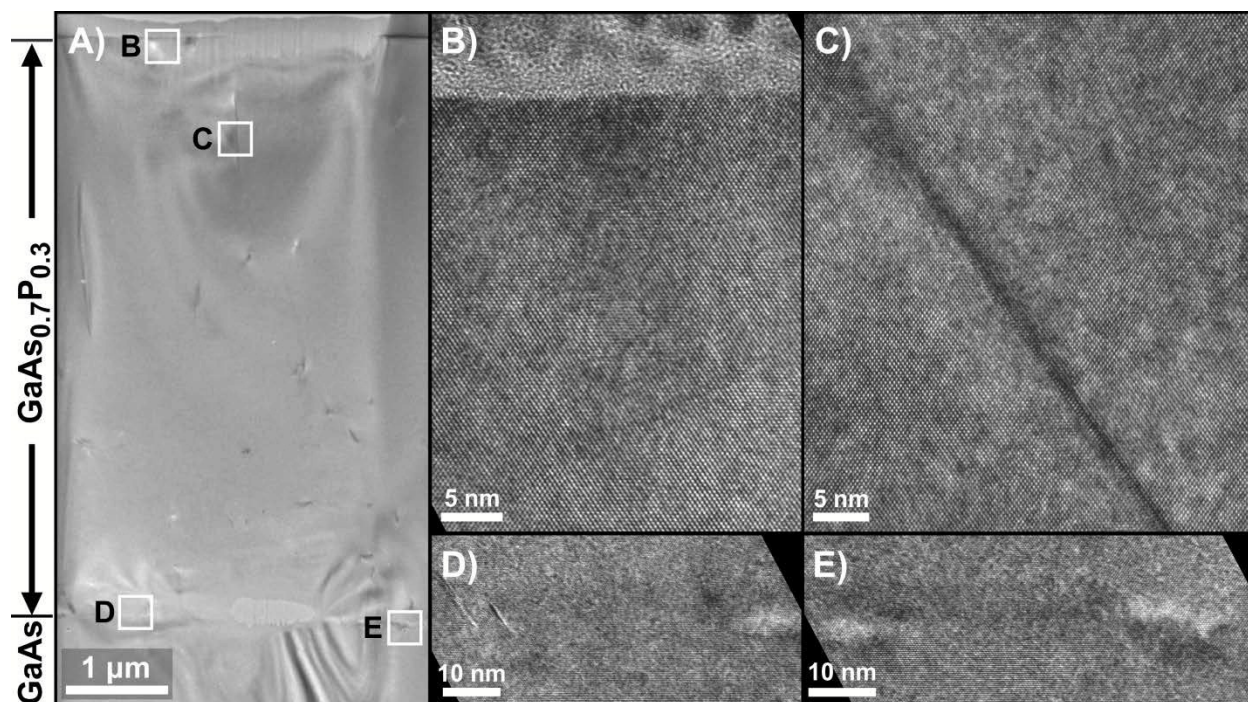


**Figure 7:** TEM of sample T10 FIB cross-section A) Overview of cross-section showing entire thickness of  $\text{GaAs}_{0.7}\text{P}_{0.3}$  film with few defects. The interface with the GaAs substrate is marked. B) HR-TEM of the surface showing no defects. C) HR-TEM of a dislocation. D and E) HR-TEM of interface showing no obvious threading dislocations and only few interfacial defects likely related to surface contamination.

### Electronic Characterization

After characterization of their physical properties, the  $\text{GaAs}_{1-x}\text{P}_x$  samples grown on  $n^+$ -GaAs substrates were cleaved and fabricated into electrodes for PEC characterization in a standard non-aqueous ferrocene/ferrocenium redox electrolyte (Table 2).<sup>14,17,38</sup> This characterization method is advantageous for the  $\text{GaAs}_{1-x}\text{P}_x$  films, as a rectifying liquid junction avoids the difficulties associated with forming solid-state junctions on rough surfaces. Impedance spectroscopy and Mott-Schottky analysis were used to measure dopant density. For the composition series,  $N_D$  from impedance scaled with increasing [P], which is consistent with the dopant originating from the source  $n$ -GaP wafer. The  $n$ -type dopant was identified as S using TOF-SIMS. Efficient incorporation of S from the pellet source in these films is expected, given the high vapor pressure of S and previous reports of S-doped CSVT films.<sup>14</sup> For the temperature-

series samples,  $N_D$  values determined by Mott-Shottky analysis were the same within error, between  $2-4 \times 10^{17} \text{ cm}^{-3}$ . TOF-SIMS shows lower [S] ( $10^{16} - 10^{17} \text{ cm}^{-3}$ ) in both the GaP wafer used for the pellet source for this series and in resulting films. Results of TOF-SIMS analysis on selected  $\text{GaAs}_{1-x}\text{P}_x$  films and both GaP source wafers can be found in Table S2.

**Table 2:** PEC  $J$ - $E$  and impedance measurement results.

	Sample	$N_D$ ( $\text{cm}^{-3}$ )	$J_{SC}$ ( $\text{mA cm}^{-2}$ )	$V_{OC}$ (V vs $E_{sol}$ )	$L_D$ (nm)
<b>Variable Composition</b>	C1	$2.1 \pm 0.8 \times 10^{17}$	$4.7 \pm 0.2$	$-0.94 \pm 0.03$	$160 \pm 30$
	C2	$2.6 \pm 0.6 \times 10^{17}$	$3.9 \pm 0.2$	$-1.02 \pm 0.02$	$140 \pm 20$
	C3	$2.7 \pm 0.5 \times 10^{17}$	$2.7 \pm 0.6$	$-1.098 \pm 0.007$	Indirect $E_g$
	C4	$3.7 \pm 0.3 \times 10^{17}$	$2.1 \pm 0.1$	$-1.09 \pm 0.02$	Indirect $E_g$
	C5	$5 \pm 3 \times 10^{17}$	$1.4 \pm 0.3$	$-1.10 \pm 0.02$	Indirect $E_g$
<b>Variable Temperature</b>	T1	$3 \pm 1 \times 10^{17}$	$5.1 \pm 0.4$	$-0.96 \pm 0.02$	$220 \pm 10$
	T2	$3.1 \pm 0.2 \times 10^{17}$	$5.3 \pm 0.3$	$-0.941 \pm 0.008$	$141 \pm 7$
	T3	$3.0 \pm 0.1 \times 10^{17}$	$6.4 \pm 0.2$	$-0.93 \pm 0.01$	$260 \pm 10$
	T4	$2.9 \pm 0.8 \times 10^{17}$	$6.1 \pm 0.5$	$-0.90 \pm 0.01$	$210 \pm 10$
	T5	$2.1 \pm 0.2 \times 10^{17}$	$6.1 \pm 0.4$	$-0.96 \pm 0.01$	$220 \pm 20$
	T6	$4.0 \pm 0.4 \times 10^{17}$	$5.8 \pm 0.3$	$-0.877 \pm 0.008$	$160 \pm 20$
	T7	$2 \pm 1 \times 10^{17}$	$6.7 \pm 0.3$	$-0.93 \pm 0.01$	$240 \pm 20$

\*All values are averages of three electrodes; errors were determined from one standard deviation.

Representative illuminated  $J$ - $E$  curves for the composition series are shown in Figure 8A. All films show higher open-circuit potentials than GaAs in the same solution due to the larger band gap of all compositions of  $\text{GaAs}_{1-x}\text{P}_x$ , consistent with older results on MOCVD grown  $\text{GaAs}_{1-x}\text{P}_x$ .<sup>46</sup> The short-circuit current  $J_{SC}$  (defined in this case as the current measured when the semiconductor potential is equal to the contacting solution potential) decreases with increasing [P]. This is the result of a number of factors. Increasing [P] increases  $E_g$ , decreasing the wavelengths which are absorbed, and for  $[P] \geq 44\%$ , the band gap becomes indirect. Additionally, increasing dopant density decreases mobility and diffusion length, which leads to increased bulk recombination and the lower  $J_{SC}$  of the higher [P] samples. Representative  $J$ - $E$  curves for the temperature series are shown in Figure 8B. The samples with  $T_{src} = 900 \text{ }^\circ\text{C}$  showed the best electronic characteristics individually and overall, indicating good reproducibility (the first sample of this series showed a much lower  $J_{SC}$ , possibly as a result of its compositional inhomogeneity). The higher growth temperature sample ( $T_{src} = 950 \text{ }^\circ\text{C}$ ) showed the same  $V_{OC}$  but

lower  $J_{SC}$ ; lower growth temperature samples showed smaller  $V_{OC}$  values as well as reduced  $J_{SC}$ . All samples showed a slight bias-dependence in light-limited photocurrent; however, dark  $J-E$  curves showed no shunting in reverse bias.

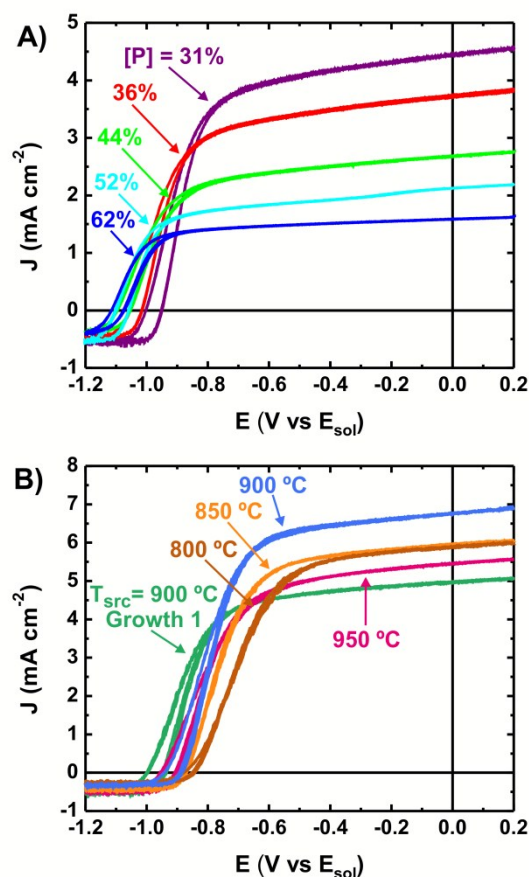


**Figure 8:** Representative JV curves. **A)** The decrease in  $J_{SC}$  across the composition series with increasing  $[P]$  is consistent with increasing  $E_g$  and the shift from direct to indirect  $E_g$ . **B)** The temperature series shows the best  $J-E$  characteristics for the samples grown at 900 °C; samples T3 and T5 have similar characteristics to T7 and therefore are omitted here. The compositional inhomogeneity of sample T1 (30.2%) appears to have reduced  $J_{SC}$ .

The spectral response of the GaAs<sub>1-x</sub>P<sub>x</sub> samples was also measured to estimate minority carrier diffusion length,  $L_D$ . External quantum efficiencies were converted to internal quantum efficiencies ( $\Phi_{int}$ ) using the measured reflectance for each sample using  $\Phi_{ext} = \Phi_{int}[1-R(\lambda)]$ . Photons with energies near  $E_g$  are absorbed deeper in the semiconductor than higher energy photons, causing  $\Phi_{int}$  to decay to zero at the band edge. This phenomenon allows  $\Phi_{int}$  to be

modelled using the Gärtner equation, which assumes that there is no recombination in the depletion region (width  $W$ ), and that  $L_D$  governs bulk recombination:<sup>47</sup>

$$\Phi_{int} = \left(1 - \frac{e^{-\alpha(\lambda)W}}{1 + \alpha(\lambda)L_D}\right) \quad (4)$$

Because there are no literature reports on the values of the absorption coefficient  $\alpha(\lambda)$  for the full range of [P] in GaAs<sub>1-x</sub>P<sub>x</sub>, values of  $\alpha(\lambda)$  at the band edge for the direct  $E_g$  compositions were estimated based on literature values of  $\alpha(\lambda)$  for two compositions; details are discussed in the SI.<sup>48</sup>  $L_D$  was not extracted for the samples with [P]  $\geq$  44% as these samples have indirect band gaps and literature values of  $\alpha(\lambda)$  were not readily available. The experimental values of  $\Phi_{int}$  as well as the results of the Gärtner fits for the data can be seen in Figure 9; the diffusion length  $L_D$  is given for each sample in Table 2. The low observed  $\Phi_{int}$  (and correspondingly low  $L_D$ ) for all samples over 500-700 nm is expected to be a result of micro-twins and threading and misfit dislocations in the films as a result of the lattice mismatch from the GaAs substrate.<sup>49</sup> The use of a compositionally graded buffer layer, which is normally employed in other growth methods, should improve electronic properties.<sup>24</sup> Overall,  $L_D$  is seen to decrease with increasing [P] (Figure 9B), as expected due to decreasing hole mobility and increasing lattice mismatch from the substrate. For the variable temperature series, the samples with  $T_{src} = 900$  °C show the best  $L_D$ , with decreased  $L_D$  for all other samples, consistent with their  $J$ - $E$  characteristics.

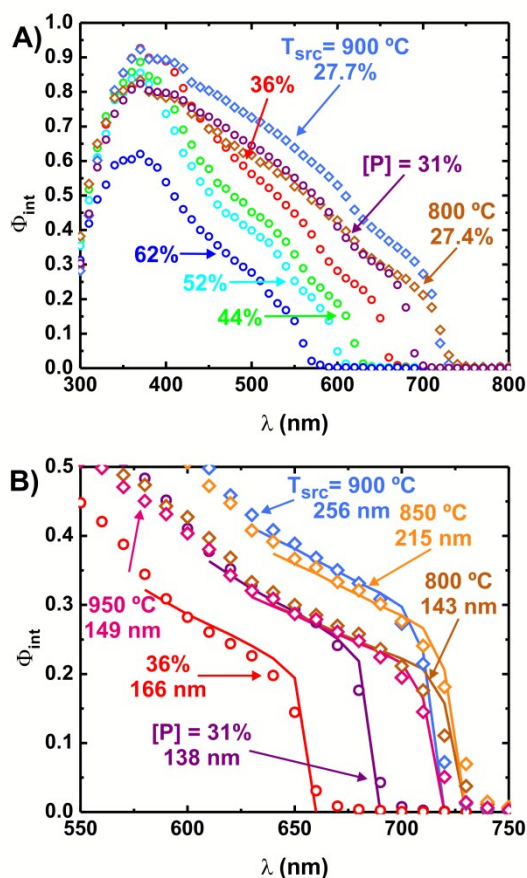


**Figure 9:**  $\Phi_{\text{int}}$  data for **A)** the composition series and **B)** representative samples of the temperature series; due to similarity, the other temperature series samples are omitted for clarity. The Gartner fits to the band edge are shown as solid lines in **B)**.

As part of the temperature series, three  $\text{GaAs}_{1-x}\text{P}_x$  samples (T8-T10) were grown on undoped GaAs substrates at a single growth condition,  $T_{\text{src}} = 900\text{ }^\circ\text{C}$ , for Hall measurements. All films were *n*-type with dopant densities in agreement with electrochemical impedance and TOF-SIMS measurements. The Hall electron mobility  $\mu_e$  was  $1200 \pm 300\text{ cm}^2\text{ V}^{-1}\text{ s}^{-1}$  (see Table S4). While there are few comprehensive measurements of  $\mu_e$  for  $\text{GaAs}_{1-x}\text{P}_x$  in the literature, these values are consistent with measurements by Tietjen and Amick, who reported  $\sim 3000\text{ cm}^2\text{ V}^{-1}\text{ s}^{-1}$  for  $\text{GaAs}_{1-x}\text{P}_x$  with  $0\% \leq [\text{P}] \leq 20\%$  at a similar dopant density in their study of various  $\text{GaAs}_{1-x}\text{P}_x$  compositions grown using HVPE. They note that there is no notable decrease in  $\mu_e$  relative to GaAs until  $[\text{P}] > 30\%$ .<sup>50</sup>

Overall, the electronic quality of GaAs<sub>1-x</sub>P<sub>x</sub> grown using CSVT is promising, but leaves room for improvement; this is especially evident in the decreased  $J_{SC}$  of all film compositions compared to MOCVD- or MBE-grown materials which utilize compositional buffers.<sup>46,51-53</sup> The volume density of misfit dislocations, for example, increases with increasing lattice mismatch between film and substrate, and therefore will exert a larger negative influence on films with higher [P]. The development of a method for compositional grading by CSVT or the implementation of defect trapping using micro- or nanostructuring of the substrate-film interface should help reduce crystalline defects, and therefore improve the electronic quality in future material.  $N_D$  across both the series is higher than  $N_D = 10^{15} \text{ cm}^{-3}$  used, for example, in the study by Gronet and Lewis, where  $J_{SC}$  up to  $\sim 15 \text{ mA cm}^{-2}$  for [P] = 30% was reported.<sup>46</sup> Performance could thus likely also be improved by optimization of the source composition and reactor to lower the carrier concentration. Finally, the incorporation of adventitious microstructures (Figure 6) resulting from particulate transfer from the source could also contribute to a decreased  $\mu_e$  and  $L_D$ , ultimately impacting  $J_{SC}$  and  $V_{OC}$ . These could be minimized by high-temperature pre-annealing of the source pellet to effectively sinter the particulate source and minimize free particulates that can transfer to the substrate during the growth process. Oxygen-related defects directly related to the H<sub>2</sub>O used as a transport agent might also reduce electronic quality, though more study would be needed to confirm this hypothesis. Chloride transport agents might be used to eliminate these defects, while maintaining very high source utilization characteristic of the CSVT process.

## Conclusion

GaAs<sub>1-x</sub>P<sub>x</sub> films with 25% ≤ [P] ≤ 65% were grown heteroepitaxially on GaAs substrates using CSVT from combined GaAs and GaP powders. XRD and EDS were used to confirm epitaxy and show excellent P incorporation in the films over a range of temperatures. The electronic properties of the materials,  $J_{SC}$ ,  $V_{OC}$ , and  $N_D$ , were measured using PEC and indicate reasonable electronic quality. These results represent an important step toward the utilization of CSVT to grow more-complicated device architectures, such as tandem photovoltaic or photoelectrochemical devices requiring ternary III-V compositions. Further improvements to the growth process, including elimination of particulate transfer during growth *via* a pre-growth sintering process, a shift to halide transport agents, the use of compositionally graded buffer layers, and better control over the carrier concentration would substantially improve the electronic properties of CSVT GaAs<sub>1-x</sub>P<sub>x</sub>, paving the way for incorporation of this material in new low-cost tandem PV or PEC concepts.

### Acknowledgements

This study was funded by the Department of Energy SunShot Initiative BRIDGE program (DE-EE0005957) and by the Research Corporation for Scientific Advancement through a Scialog Award. A.L.G. acknowledges support from a NSF Graduate Research Fellowship (DGE-0829517). We acknowledge the use of the CAMCOR shared instrument facility at the University of Oregon, which is supported by grants from the M.J. Murdock Charitable Trust, the W. M. Keck Foundation, ONAMI, and the NSF. Work at the Molecular Foundry was supported by the Office of Science, Office of Basic Energy Sciences, of the U.S. Department of Energy under Contract DE-AC02-05CH11231. We thank Kurt Langworthy, Dr. Stephen Golledge,

Robert Fischer, Joshua Razink, Matthew Kast, Dr. Adam Smith, Michaela Burke, Lisa Enman and Benjamin Bachman for their support on this project. In memory of T.J. Mills.

## References

- 1 J. Jean, P. R. Brown, R. L. Jaffe, T. Buonassisi and V. Bulović, *Energy Environ. Sci.*, 2015, **8**, 1200–1219.
- 2 M. G. Walter, E. L. Warren, J. R. McKone, S. W. Boettcher, Q. Mi, E. A. Santori and N. S. Lewis, *Chem. Rev.*, 2010, **110**, 6446–73.
- 3 P. Dutta, in *Comprehensive Semiconductor Science and Technology*, eds. P. Bhattacharya, R. Fornari and H. Kamimura, Elsevier, Boston, 1st edn., 2011, pp. 36–80.
- 4 O. D. Miller, E. Yablonovitch and S. R. Kurtz, *IEEE J. Photovoltaics*, 2012, **2**, 303–311.
- 5 S. R. Kurtz, P. Faine and J. M. Olson, *J. Appl. Phys.*, 1990, **68**, 1890–1895.
- 6 J. F. Geisz and D. J. Friedman, *Semicond. Sci. Technol.*, 2002, **17**, 769–777.
- 7 S. Tomasulo, K. N. Yaung and M. L. Lee, *IEEE J. Photovoltaics*, 2012, **2**, 56–61.
- 8 M. A. Green, K. Emery, Y. Hishikawa, W. Warta and E. D. Dunlop, *Prog. Photovoltaics Res. Appl.*, 2015, **23**, 1–9.
- 9 O. Khaselev and J. Turner, *Science*, 1998, **280**, 425–427.
- 10 M. Woodhouse and A. Goodrich, *NREL/PR-6A20-60126*, 2013.
- 11 B. A. Pinaud, J. D. Benck, L. C. Seitz, A. J. Forman, Z. Chen, T. G. Deutsch, B. D. James, K. N. Baum, G. N. Baum, S. Ardo, H. Wang, E. Miller and T. F. Jaramillo, *Energy Environ. Sci.*, 2013, **6**, 1983–2002.
- 12 F. H. Nicholl, *J. Electrochem. Soc.*, 1963, **110**, 1165–1167.
- 13 G. Perrier, R. Philippe and J. P. Dodelet, *J. Mater. Res.*, 1988, **3**, 1031–1042.
- 14 A. J. Ritenour, J. W. Boucher, R. DeLancey, A. L. Greenaway, S. Aloni and S. W. Boettcher, *Energy Environ. Sci.*, 2015, **8**, 278–285.
- 15 J. W. Boucher, A. J. Ritenour, A. L. Greenaway, S. Aloni and S. W. Boettcher, *Proc. 40th IEEE Photovolt. Spec. Conf.*, 2014, **40**, 0460–0464.
- 16 J. W. Boucher, A. J. Ritenour and S. W. Boettcher, *Proc. SPIE*, 2013, **38**, 87250Z.
- 17 A. J. Ritenour, R. C. Cramer, S. Levinrad and S. W. Boettcher, *ACS Appl. Mater. Interfaces*, 2012, **4**, 69–73.

- 18 A. J. Ritenour and S. W. Boettcher, *Proc. 38th IEEE Photovolt. Spec. Conf.*, 2012, **36**, 913–917.
- 19 T. J. Grassman, A. M. Carlin, J. Grandal, C. Ratcliff, L. Yang, M. J. Mills and S. A. Ringel, *Proc. SPIE*, 2012, **8256**, 82560R.
- 20 H. Liu, Z. Ren, Z. Liu, A. G. Aberle, T. Buonassisi and I. M. Peters, *Opt. Express*, 2015, **23**, A382–A390.
- 21 H. Döscher, J. F. Geisz, T. G. Deutsch and J. A. Turner, *Energy Environ. Sci.*, 2014, **7**, 2951–2956.
- 22 S. Hu, C. Xiang, S. Haussener, A. D. Berger and N. S. Lewis, *Energy Environ. Sci.*, 2013, **6**, 2984–2993.
- 23 G. W. Wicks, in *Handbook of Photonics*, ed. M. C. Gupta, CRC Press, New York, 1st edn., 1997, pp. 5–23.
- 24 M. J. Mori, S. T. Boles and E. A. Fitzgerald, *J. Vac. Sci. Technol. A Vacuum, Surfaces, Film.*, 2010, **28**, 182–188.
- 25 G. B. Stringfellow, *J. Cryst. Growth*, 1983, **62**, 225–229.
- 26 T. Fukui and N. Kobayashi, *J. Cryst. Growth*, 1985, **71**, 9–11.
- 27 P. H. Robinson, *RCA Rev.*, 1963, 574–584.
- 28 G. E. Gottlieb, *J. Electrochem. Soc.*, 1965, **112**, 192–196.
- 29 R. K. Purohit, *J. Mater. Sci.*, 1968, **3**, 330–332.
- 30 G. E. Gottlieb and J. F. Corboy, *RCA Rev.*, 1963, **24**, 585–595.
- 31 M. G. Mauk, B. W. Feyock and J. E. Cotter, *J. Cryst. Growth*, 2001, **225**, 528–533.
- 32 M. G. Mauk, A. N. Tata and B. W. Feyock, *J. Cryst. Growth*, 2001, **225**, 359–365.
- 33 P. Sharma, M. T. Bulsara and E. A. Fitzgerald, *ECS Trans.*, 2010, **33**, 843–848.
- 34 H. Q. Hou, B. W. Liang, T. P. Chin and C. W. Tu, *Appl. Phys. Lett.*, 1991, **59**, 292–294.
- 35 P.-A. Hoss, L. A. Murray and J. J. Rivera, *J. Electrochem. Soc. Solid State Sci.*, 1968, **115**, 553–556.
- 36 J. F. Geisz, J. M. Olson, M. J. Romero, C. S. Jiang and A. G. Norman, *Conf. Rec. 2006 IEEE 4th World Conf. Photovolt. Energy Conversion, WCPEC-4*, 2007, **1**, 772–775.

- 37 R. G. Wilson, F. A. Stevie and C. W. Magee, *Secondary ion mass spectrometry: a practical handbook for depth profiling and bulk impurity analysis*, Wiley, New York, 1989.
- 38 A. J. Ritenour, S. Levinrad, C. Bradley, R. C. Cramer and S. W. Boettcher, *ACS Nano*, 2013, **7**, 6840–6849.
- 39 L. G. Casagrande, A. Juang and N. S. Lewis, *J. Phys. Chem. B*, 2000, **104**, 5436–5447.
- 40 S. M. Sze, *Physics of Semiconductor Devices*, John Wiley & Sons, New York, 1981.
- 41 L. J. Van der Pauw, *Phillips Tech. Rev.*, 1958, **20**, 220–224.
- 42 W. Sun, Y. Guo, H. Xu, Z. Liao, Q. Gao, H. H. Tan, C. Jagadish and J. Zou, *J. Phys. Chem. C*, 2013.
- 43 G. B. Stringfellow, *Organometallic Vapor-Phase Epitaxy*, Academic Press, New York, 2nd ed., 1999.
- 44 B. A. Lombos, D. Côté, J. P. Dodelet, M. F. Lawrence and J. I. Dickson, *J. Cryst. Growth*, 1986, **79**, 455–462.
- 45 S. Kishino, M. Ogirima and K. Kurata, *J. Electrochem. Soc. Solid State Sci. Technol.*, 1972, **119**, 7–12.
- 46 C. M. Gronet and N. S. Lewis, *Nature*, 1982, **300**, 733–735.
- 47 W. W. Gärtner, *Phys. Rev.*, 1959, **116**, 84–87.
- 48 S. Hasegawa, A. Tanaka and T. Sukegawa, *J. Appl. Phys.*, 1984, **55**, 3188–3189.
- 49 J. B. McNeely and A. M. Barnett, *Conf. Rec. IEEE Photovoltaics Spec. Conf.*, 1984, 1414–1415.
- 50 J. J. Tietjen and J. A. Amick, *J. Electrochem. Soc.*, 1966, **113**, 724–728.
- 51 T. J. Grassman, M. R. Brenner, M. Gonzalez, A. M. Carlin, R. R. Unocic, R. R. Dehoff, M. J. Mills and S. A. Ringel, *IEEE Trans. Electron Devices*, 2010, **57**, 3361–3369.
- 52 S. Tomasulo, K. Nay Yaung, J. Simon and M. L. Lee, *Appl. Phys. Lett.*, 2012, **101**, 033911.
- 53 C. M. Gronet and N. S. Lewis, *J. Phys. Chem.*, 1984, **88**, 1310–1317.